Nonlinear Analysis 71 (2009) e1807–e1817

Contents lists available at ScienceDirect

Nonlinear Analysis

journal homepage: www.elsevier.com/locate/na

Effects on acoustics caused by ocean solitons, Part A: Oceanography

A. Warn-Varnas [a,*], S.A. Chin-Bing [a], D.B. King [a], J. Hawkins [b], K. Lamb [c]

[a] *Naval Research Laboratory, Stennis Space Center, MS 39529, USA*

[b] *Planning Systems Inc., Slidell, LA 70458, USA*

[c] *University of Waterloo, Waterloo, Ontario, Canada N2L 3G1*

ARTICLE INFO

Keywords:
Solitary waves
Model parameters
Scaling parameters
Wave amplitude
Wavelength and phase speed
Parameter space regimes
Nonhydrostatic models

ABSTRACT

Our work addresses the link between internal solitary waves and acoustics. The location of the study is in the Yellow Sea south of the Shandong peninsula. Previously in this region, we have performed internal solitary wave generation and propagation simulations with the Lamb nonhydrostatic model [K. Lamb, Numerical experiments of internal waves generated by strong tidal flow across a finite amplitude bank edge, J. Geophys. Res. 99 (c1) (1994) 848–864; A. Warn-Varnas, S.A. Chin-Bing, D.B. King, J.A. Hawkins, K.G. Lamb, M. Teixeira, Yellow Sea ocean-acoustic solitary wave modeling studies, J. Geophys. Res. 110 (2005) C08001, doi:10.1029/2004JC002801]. The model parameters were tuned to SAR data. Here, we consider variations of solitary wave characteristics in parameter space. We introduce scaling parameters for a two-layer analogue configuration. This analogue is applied to predicted numerical solutions with the full nonlinear nonhydrostatic Lamb model in the first of the above-mentioned references. Variations of density difference across the pycnocline, tidal forcing and topographic height are considered. Characteristics of solitary waves are analyzed as the parameters deviate from a tuned case to data. Changes of solitary wave functional form, amplitude, wavelength, and phase speed are tracked. We consider oceanographic and acoustical parameters that describe the physical ocean–acoustic environment and its associated variability. For certain source, receiver, and acoustical frequency configurations, a redistribution of acoustical energy to higher modes can occur and result in acoustical intensity loss in the presence of solitary wave trains [A. Warn-Varnas, S.A. Chin-Bing, D.B. King, J. A. Hawkins, K.G. Lamb, M. Teixeira, Yellow Sea internal solitary wave variability, in: N.G. Pace, Finn B. Jensen (Eds.), Impact of Littoral Environmental Variability on Acoustic Predictions and Sonar Performance, Kluwer Academic Publishers, Dordrecht, The Netherlands, 2002]. This will be considered in part B.

Published by Elsevier Ltd

1. Introduction

In the Shandong Peninsular region of the Yellow Sea internal solitary waves have been observed and modeled, Warn-Varnas, et al. [1] and Teixeira, et al. [2]. In these studies nonhydrostatic and Korteweg–de Vries (KdV) type model predictions were tuned to Synthetic Aperture RADAR (SAR) observations. The predictions encompassed the full nonlinear nonhydrostatic numerical solution of Lamb [3] and the weakly nonlinear Dnoidal solution of KdV equation of Apel [4]. The Dnoidal solution consisted of a mixture of cnoidal and cosine functions that can degenerate into cosine or sech^2 functions. The full nonlinear nonhydrostatic numerical solutions of Lamb [3] contained all possible functional forms that can evolve through nonlinear dynamics.

* Corresponding author. Tel.: +1 228 688 5223; fax: +1 228 688 4759.
E-mail address: varnas@nrlssc.navy.mil (A. Warn-Varnas).

0362-546X/$ – see front matter. Published by Elsevier Ltd
doi:10.1016/j.na.2009.02.104

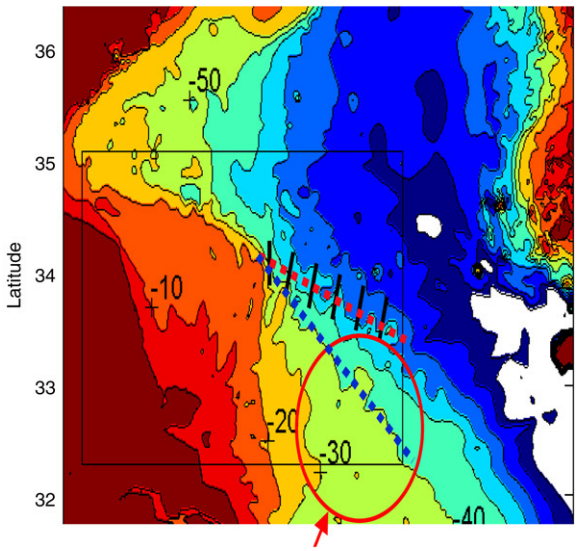

Fig. 1. Location of study region south of Shandong Peninsula in Yellow Sea. Red dotted line indicates modeling track. Black lines are SAR observations. Blue dotted line is a shallower modeling track. Red circle outlines area where Zhou et al. [7] conducted their measurements. (Color figures available online.)

Model predicted and observed solitary wave trains can be analyzed with various techniques. The KdV solution can be expressed as a linear superposition of cnoidal waves and their nonlinear interaction, Osborne [5]. Linear Fourier and wavelet analysis can be applied to solitary wave trains for deducing fundamental modes of first order nonlinear dynamics [6]. Direct scattering transform of solitary wave trains can elucidate the solitary wave train nonlinear dynamical evolution [6], as the dispersive effects cause the amplitudes and number of oscillations to vary.

In the shelfbreak area of the Shandong Peninsula, the barotropic tide interacts with topography in the presence of stratification and generates a baroclinic tide in the form of an internal bore. The internal bores propagated away from the shelfbreak, steepened through nonlinear effects and disintegrated into solitary wave trains through frequency and amplitude dispersion [1]. The resultant solitary wave trains arising from full nonlinear dynamics are complex and can exhibit changes in the functional structure [4].

The original interest in the region of the Yellow Sea south of the Shandong Peninsula started with the acoustical measurements of shallow-water sound propagation, Fig. 1. Acoustical measurements performed by Zhou et al. [7], over a period of several summers, showed an anomalous drop in acoustical intensity of about 20 dB at a range of 28 km for acoustic frequencies of around 630 Hz. The transmission loss was found to be time and direction dependent. The authors postulated the existence of solitons in the thermocline through a gated sine function representation and performed transmission loss calculations using an acoustic parabolic equation (PE) model. The simulation results from this hypothetical case showed that an anomalous transmission loss could occur at a frequency of around 630 Hz when acoustical waves and solitons interact. Computer simulations subsequently confirmed (Chin-Bing et al. [8]; King et al. [9]) that the resonant like transmission loss is caused by an acoustical mode coupling due to the presence of solitons, together with a corresponding larger bottom attenuation for the coupled acoustic modes.

A study of the interaction between several environments of propagating solitary wave trains and the acoustical field was conducted in Warn-Varnas et al. [10] and showed that, indeed, for certain frequencies a loss of acoustical intensity occurs.

A train of solitary waves can be characterized by wavelength scales of the order of 1000 m. The phase speed can be around 1 m/s, amplitudes 50 m to 250 m, and frequency of the order of 10^{-3} Hz. The individual wavelengths, amplitudes, and phase speeds vary in a solitary wave train itself and in the different regions of the world oceans where solitary waves are found. On the acoustical side we are dealing with frequencies of a few hundred to few thousand Hz. At a frequency of 1000 Hz the wavelength is 1.5 m for an ocean sound speed of 1500 m/s. The acoustical propagation speeds and frequencies are orders of magnitude higher than the corresponding oceanographic analogue.

In the range of 100 Hz to 2 kHz, the acoustical wavelengths are orders of magnitude smaller than the oceanographic counterparts. The comparably shorter acoustical wavelengths in relation to the solitary wave wavelengths enable the acoustical field to interact with the solitary wave distribution located between the source and the receiver. As a result many interactions of the acoustical field and the solitary wave train can occur. The differences in scenarios with and without solitary wave disturbances in the acoustical path can be striking.

In Part A of 'Effects on acoustics caused by ocean solitons', we consider the oceanographic parameters that describe the oceanographic fields and the associated variability of the oceanographic field. The Part A paper is divided into sections on model predictions in Shandong Peninsula region, parameter variations studies with Lamb model, dispersion and conclusion.

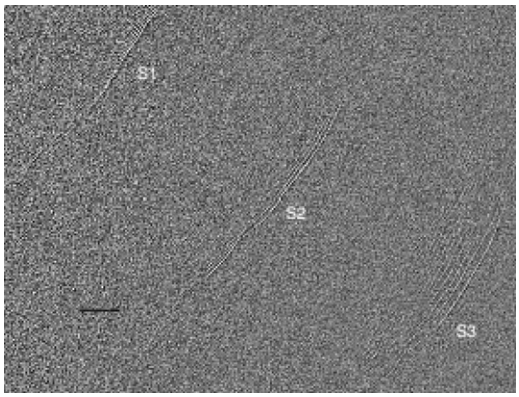

Fig. 2. RADARSAT1 observations on 8 August 1998. S1, S2, and S3 indicate a zoom of the first three solitary wave trains to propagate away from the shelfbreak along the red dotted line shown in Fig. 1. The solid black line represents a scale of 46 km.

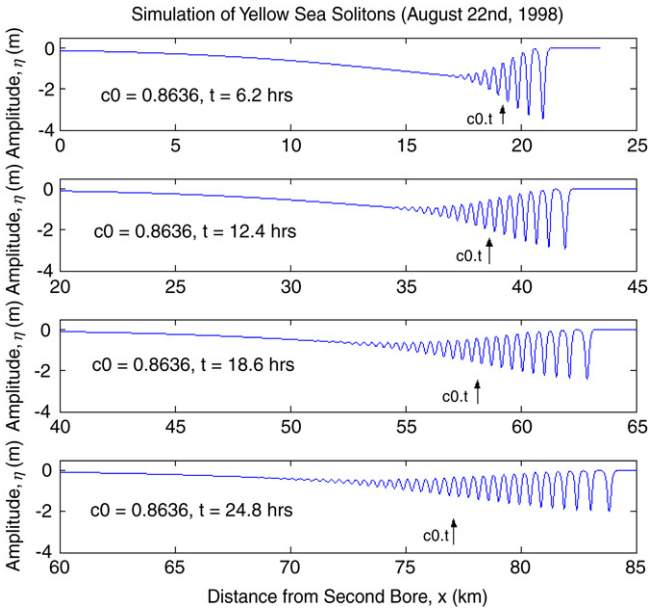

Fig. 3. Predicted solitary wave train evolution with Apel model for two tidal periods. Arrows show the centroid of the packet that moves with the linear phase speed, c_0.

2. Model predictions in Shandong Peninsula region

Along the red dotted line in Fig. 1, solitary wave trains have been observed to propagate away from the shore. An observation by RADARSAT1, Synthetic Aperture Radar (SAR), on 8 August 1998 is shown in Fig. 2. S1, S2, and S3 denote a zoom of the first three solitary wave trains. The spacing between the bright convergence lines increases as one proceeds from S1 to S3, suggesting generation in the coastal shelfbreak area. The spacing between the wave packets has a high degree of regularity along a defined direction. The overall concave shape of the wave front is preserved along the travel path, which again suggests that these internal wave packets originated from the same shelfbreak location.

In a previous study, predictions of solitary wave trains in the Shandong region were undertaken in the Shandong Peninsula region of the Yellow Sea with the Dnoidal model of Apel [4]. The simulations were along the red track shown in Fig. 1. Climatological density profiles were used for initialization and parameter estimates. A solution with parameters tuned to SAR data is shown in Fig. 3. The simulations show the evolution of a solitary wave train at 6.2 h intervals for two tidal periods. Arrows indicate the centroid of the wave packet that moves with a linear phase speed of .8636 m/s. The front of the wave packet moves with the nonlinear phase speed of .9412 m/s.

The beginning of each wave packet has flat segments after the first few depressions. This indicates a cnoidal wave. The back of the train exhibits a cosine structure. The wave train is a mixture of cnoidal and cosine waves Apel [4].

Another set of predictions was undertaken with fully nonlinear nonhydrostatic model of Lamb [3] described in the Appendix. A simulation with parameters tuned to SAR data is shown in Fig. 4 in terms of an isopycnal in mid pycnocline for

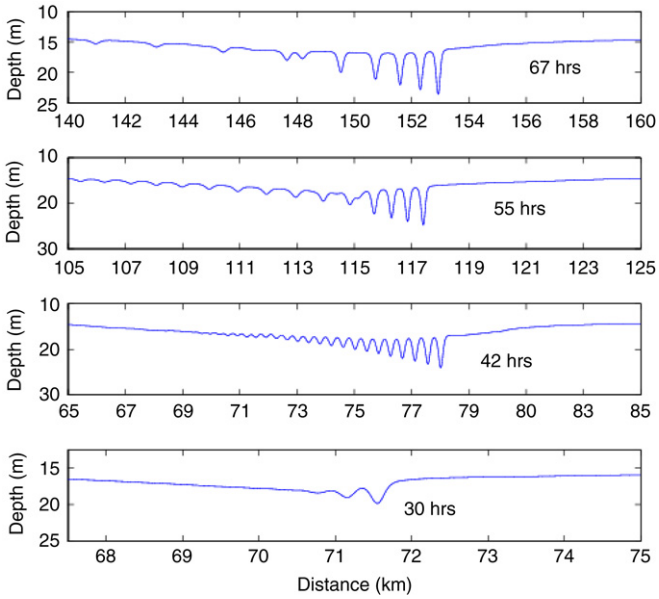

Fig. 4. Expanded view of $\sigma_t = 22.5$ isopycnal predicted with Lamb model at 30, 42, 55, and 67 h.

Table 1
Simulation parameters: h_d is the pycnocline depth, H (m) is the water depth, V_T is the tidal strength, d_H is the length of computational domain.

Case	h_d	H (m)	U_0 (m/s)	d_H (km)
1	15	70	.7	240

the second solitary wave train to come off the shelf. A change in structure of the solitary wave train can be seen in the time interval from 42 to 55 h. At 55 h the back of the train has larger wavelengths (separations between depressions) than the front of the train. This will be referred as a type B configuration. At 42 h the wavelengths decrease from front to back with the largest wavelength in front. This is the expected order and will be referred as type A configuration.

The two configurations suggest two different dynamical regimes evolving from the full nonlinear nonhydrostatic model of Lamb [3].

3. Parameter variation studies with Lamb model

3.1. Solitary wave trains in domain

The parameters for a previous simulations of oceanographic fields in the Shandong Peninsula region are listed in Table 1. These are pycnocline depth h_d, vertical depth H, tidal forcing U_0, and d_H the horizontal domain size. Case 1, in Table 1, represents a tuned set of parameters [1]. The semidiurnal tidal flow moves back and forth over the shelfbreak and generates internal bore depressions. These depressions split into right and left propagating waves. Nonlinear effects steepen the depressions and disintegration into solitary wave occurs, through frequency and amplitude dispersion. Fig. 5 illustrates the evolution of solitary wave trains as the tide interacts with topography in the presence of stratification. Fig. 5(a) shows the initial off-bank flow generating depressions. In Fig. 5(b) a solitary wave train is forming at about 25 km. The depression at 50 km is the off-shelf propagating depression formed to the lee of the ridge during the first tidal period. It disintegrates into solitary waves in time, Fig. 5(c). Each semidiurnal tidal period, 12.4 h, a solitary wave train is formed. Fig. 5(d) is 24 h apart from Fig. 5(c) and contains 2 additional solitary wave trains.

3.2. Variation of solitary wave characteristics in parameter space

The model predictions are conducted with a pycnocline located at 15 m, Table 1 and Fig. 5. Case 1 in Table 1 is initialized from density profiles derived from climatology and observations. The predicted solitary wave trains evolve into two configurations, A and B discussed in Section 2.

Here, we perform a study of solitary wave train characteristics dependence on density difference across the pycnocline, barotropic tidal forcing and topographic height variations. We introduce scaling parameters for a two-layer analogue with

Table 2
Characterization study parameters. $h_1 = 15$ m and $h_2 = 55$ m for cases 1–6; $h_1 = 25$ m and $h_2 = 45$ m for case 7; $L_T = 5674$ m, $\mu = .41$.

Case	$\Delta\rho$	c_0 (m/s)	F	δ	L_M (m)	ε_b	ε	U_0 (m/s)
1	.0037	0.66	1.06	2.3×10^{-4}	4973	.79	.70	.7
2	.0060	0.83	0.84	1.4×10^{-4}	4973	.79	.70	.7
3	.0016	0.43	1.63	5.3×10^{-4}	4973	.79	.70	.7
4	8.7×10^{-4}	0.32	2.2	9.7×10^{-4}	4973	.79	.70	.7
5	8.7×10^{-5}	0.10	7.0	9.7×10^{-3}	4973	.79	.70	.7
6	.0037	0.66	0.46	2.3×10^{-4}	2131	.79	.30	.3
7	.0037	0.66	1.06	2.3×10^{-4}	4973	.64	.56	.7

the mid pycnocline, at 15 m, separating the layers:

$$\Delta_\rho = (\rho_2 - \rho_1)/\rho_2,$$
$$c_0 = \left[\frac{g\Delta_\rho h_1}{1 + \frac{h_1}{h_2}}\right]^{1/2},$$
$$\delta = (\sigma H/c_0),$$
$$F = \frac{U_0}{c_0},$$
$$L_M = \frac{U_0}{\sigma},$$
$$L_T = \frac{r(x)}{r(x)'},$$
$$\gamma = \frac{c_0}{\sigma L_T},$$
$$\mu = \left[\frac{f}{\sigma}\right]^2,$$
$$\varepsilon_b = \frac{h_T}{H},$$
$$\varepsilon = \frac{L_M}{L_T}\varepsilon_b.$$

ρ_1 and ρ_2 are layer densities; h_1 is the upper layer thickness; h_2 is the lower layer thickness; H is the depth; L_T is the topographic length scale; $r(x) = H - h(x)$ where $h(x)$ is the topographic height with h_T maximum; L_M is the tidal excursion distance; c_0 is the phase speed; δ is the nonhydrostatic dispersion parameter; F is the Froude number; μ is the Coriolis dispersion; f is the Coriolis parameter; σ is the tidal frequency; U_0 is the barotropic tide.

Similar scaling parameters are used in Gerkema [11] and Lamb [3], where L_M, is the tidal excursion and L_T, the topographic length scale parameters are defined. For the topographic length scale, L_T, the maximum value will be used. Topography is simplified, for this study, by removing the small mount or finger that appears in Fig. 5. Table 2 lists parameters of study.

Case 1 in Table 2 is equivalent to case 1 in Table 1 with the topography finger removed. Results are similar. Case 1 in Table 2 is the basic reference case of this parameter variation study. Fig. 6 shows predicted density at 55 h. There are 4 evolved solitary wave trains propagating away from the shelfbreak. Other solitary wave trains are forming off the shelf. On the shelf there are solitons of elevation. An enlargement of the second solitary wave train is shown in the lower panel of Fig. 6. The leading soliton is located at 119 km in range. When the previous topography, containing the finger, is used the location is at 117.5 km, Fig. 4. The train consists of separated solitons with the spacing between them tending to increase towards the back of the train, indicative of category B behavior [1]. Category A being a behavior where the separation between solitons decreases towards the back. Table 2 indicates parameters of this case using a two-layer model estimate with interface located at pycnocline, 15 m. Estimated phase speed, c_0, is .66 m/s, L_M, tidal excursion distance is 4973 m, L_T, horizontal length scale is 5674 m, Froude number is 1.06, δ, nonhydrostatic dispersion parameter is 2.3×10^{-4}, h_T, height of topography is 55 m, ε, parameter of nonlinearity is .70. The internal tide is disintegrated into solitary waves. The Froude number is near critical, nonhydrostatic dispersion has a small magnitude that is indicative of a tide that has disintegrated into solitary waves [11].

Case 2 in Table 2 has a larger density jump across the pycnocline. This leads to solitary wave trains travelling further down range, relative to case 1, with a higher phase speed. With the larger density jump, the nonhydrostatic dispersion parameter and the Froude number are lower.

Cases 3, 4, and 5, Table 2, have progressively lower density jumps across the pycnocline. As the density jump decreases, the phase speed decreases, Froude number increases, and nonhydrostatic dispersion parameter increases. Parameters of topographic height and nonlinearity stay at the same level as for cases 1 and 2. Fig. 7 shows the predicted solitary waves trains for case 4, Table 2, at 55 h. The solitary wave trains are not as far down range as those of case 1 in Fig. 6, indicative of a lower phase speed, $c_0 = .32$ m/s instead of $c_0 = .66$ m/s for case 1. There are fewer solitons in the second train relative to case 1, Figs. 7 and 6. In the second train, Fig. 7, the separation between solitons increases from front to back of the train. The first soliton in the train is much wider than the other solitons of the train. In case 1 the first soliton has a comparable

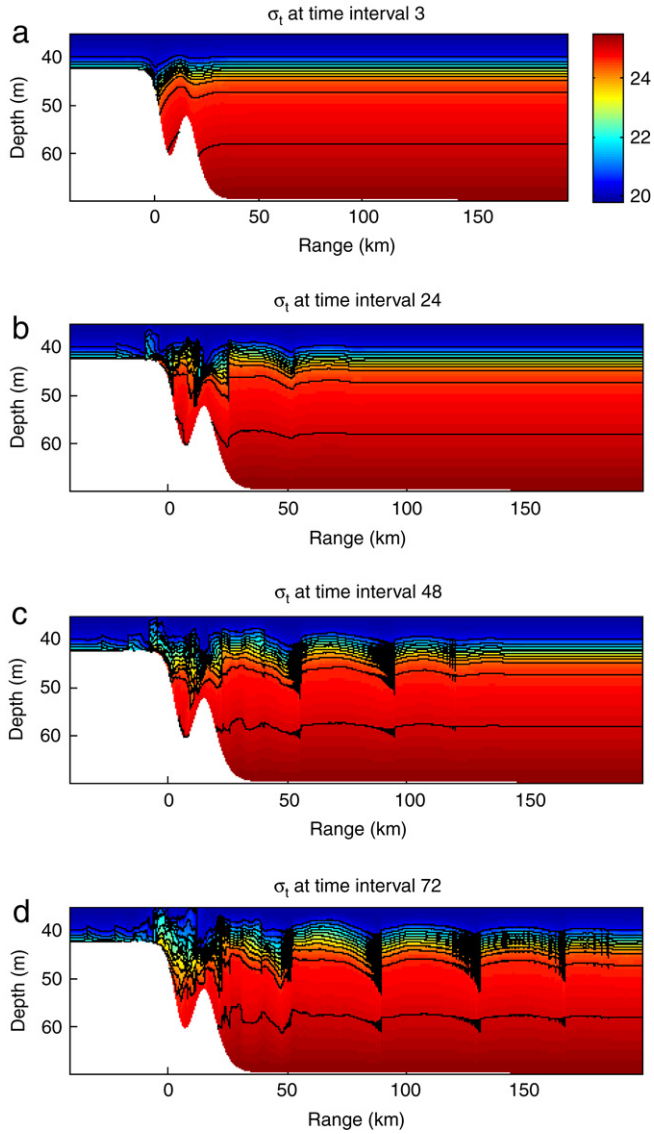

Fig. 5. Oceanographic model simulations with tuned parameters, case 1 in Table 1. These simulations will be used for acoustical studies. Shown are σ_t density fields at hours (a) 3, (b) 24, (c) 48, and (d) 72. Labeling is from top to bottom.

width to solitons behind it. The larger width for the first soliton appears as the density difference across the pycnocline is decreased. Also, the amplitude of the first soliton increases relative to case 1. The weaker stratification of case 4 leads to large amplitudes.

As the stratification across the pycnocline decreases further, case 5 in Table 2, more changes occur. The density difference across the pycnocline is now weak, the weakest in a set of parameter variations. The phase speed is the lowest among the cases in Table 2. Froude number and nonhydrostatic parameter are the largest among the cases. The predicted density structure undergoes a profound change. At 95 h, Fig. 8, there are no solitary wave trains. The movement of the semidiurnal (M2) tide causes a depression and lifting of the isopycnals across the shelfbreak. Small depressions of isopycnals that propagate to the right are visible off the shelfbreak. They are suggestive of Lee waves induced by tidal flow to the right. There are indications of nonlinear steepening that does not evolve into solitary wave trains.

Cases 6 and 7 in Table 2 involve variations of barotropic tidal forcing and topographic height relative to case 1. In case 6 the barotropic tidal forcing is reduced from .7 m/s to .3 m/s, Table 2. The Froude number, tidal excursion and nonlinearity parameters decrease relative to case 1. A decrease of barotropic tidal forcing results in internal bores of smaller amplitudes, Figs. 9 and 6. The internal bores of smaller amplitude evolve into smaller amplitude solitary wave trains, Figs. 9 and 6. In Fig. 9 there is no evolved solitary wave train at around 140 km (not shown) that relates to the Lee wave formed during initial off-shelf flow. The three visible trains in Fig. 9 have fewer solitons and less amplitude than those of Fig. 6. Less

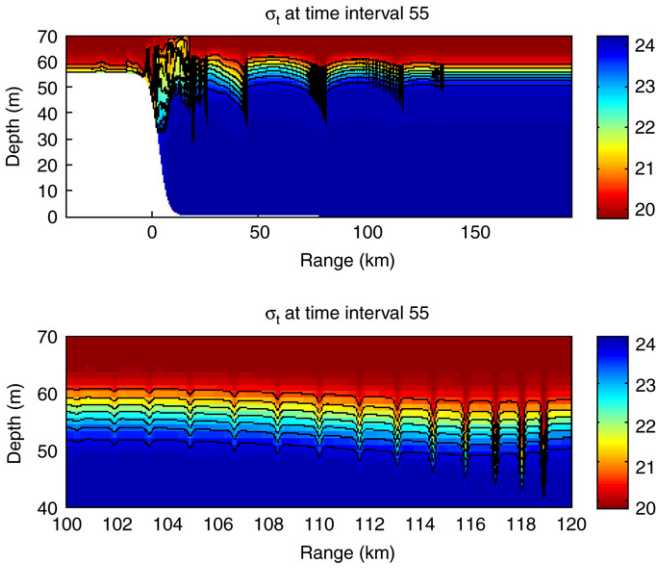

Fig. 6. Case 1 in Table 2. This is an analogue of case 1 in Table 1 with the finger in topography removed. Predicted density field at 55 h. Upper panel shows predicted density structure. Lower panel shows an expanded view of second solitary wave train.

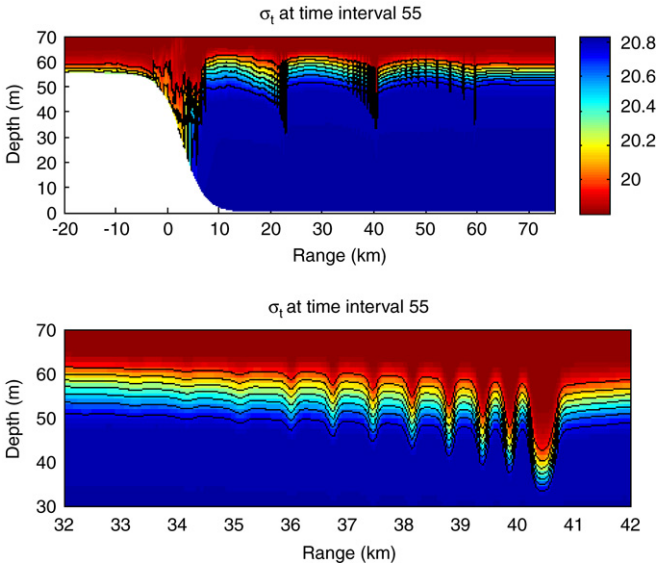

Fig. 7. Case 4 in Table 2. Predicted density field at 55 h. Upper panel shows predicted density structure. Lower panel shows an expanded view of second solitary wave train. Case 4 has a lower density difference across the pycnocline relative to case 1.

barotropic tidal forcing results in a weaker interaction with topography and a weaker internal tide that leads to different solitary wave characteristics.

In case 7 the topographic height is decreased from 55 m to 45 m relative to case 1, Table 2. For this case the topographic height and nonlinearity parameters decrease relative to case 1, Table 2. Fig. 10 shows the density prediction at 55 h. On the shelf there is reflectance off the left boundary that causes difference in structure from case 1.The number of solitary wave trains off the shelf is the same as in Fig. 6. In the second train the number of solitary waves has decreased and the amplitudes of the solitons are smaller. Lowering of topographic height results in fewer solitons with less amplitude. The dynamics is less nonlinear, as suggested by decrease of nonlinear parameter ε. The dynamics can also be less nonlinear, for the same nonlinear parameter ε, as the density difference across the layers tends to zero ($\Delta_\rho \rightarrow 0$), cases 1 and 5 in Table 2. This arises because of decreased energy transfer into the baroclinic internal tide, from barotropic tide interaction with topography in the presence of weaker stratification.

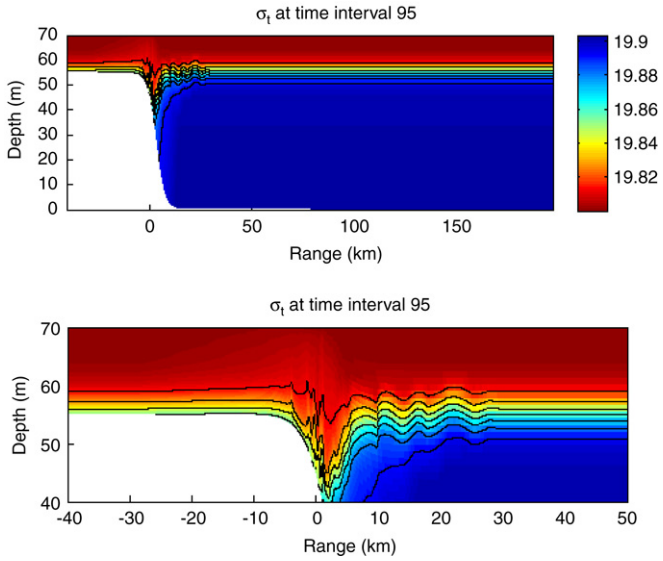

Fig. 8. Case 5 in Table 2. Case 5 has a ten times lower density difference across the pycnocline relative to case 4. Predicted density field at 95 h. Upper panel shows predicted density structure. Lower panel shows an expanded view of second solitary wave train. Note the absence of solitary wave trains.

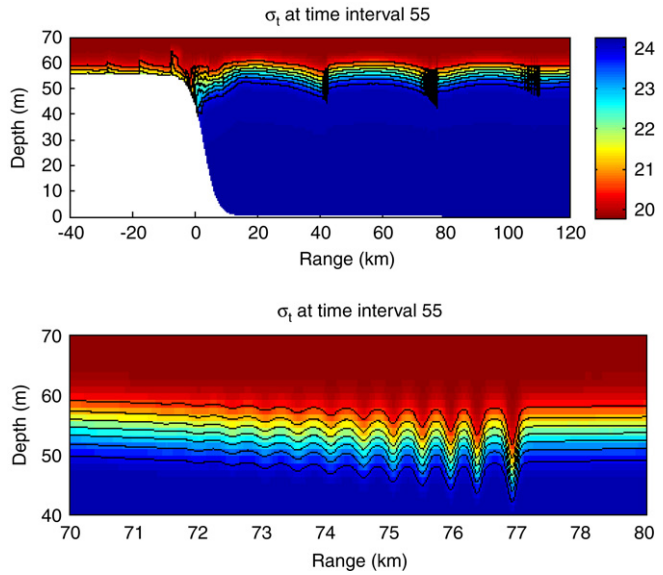

Fig. 9. Case 6 in Table 2. This case has a lower barotropic tidal forcing velocity, $U_0 = .3$ m/s, relative to case 1. Predicted density field at 55 h. Upper panel shows predicted density structure. Lower panel shows an expanded view of second solitary wave train. Note a decrease in number of solitary waves in train and their amplitudes relative to case 1.

4. Dispersion

Dispersion analysis is performed for case 1 in Table 1 (tuned to SAR data) of the second solitary wave train to come off the shelf at 30, 42, 55, and 67 h. An isopycnal of $\sigma_t = 22.5$ located in the middle of the pycnocline is chosen for tracking the solitary wave train, Fig. 4. The wavelength is defined as the distance between successive centers of troughs. Wave amplitude is defined as the vertical displacement of an isopycnal from just ahead of an individual wave. Fig. 4 shows the time evolution of the second solitary wave to come off the shelf at the respective time periods. A phase speed estimate for the first soliton was made by tracking the center of the first depression in time. A straight line fit yielded a propagation speed of 0.83 m/s. Fig. 11 shows the wavelength versus amplitude dispersion. At 30 h the amplitudes of the second soliton train vary from about 9.5 to .2 m and the wavelengths decrease from about 250 to 200 m. At 42 h the amplitudes range is slightly less and the wavelengths vary from 425 to 350 m, indicating decreasing wavelengths or less space between the centers of the depressions, from front to back of the train. The 30 and 42 h dispersions belong to regime A behavior, Section 2, where

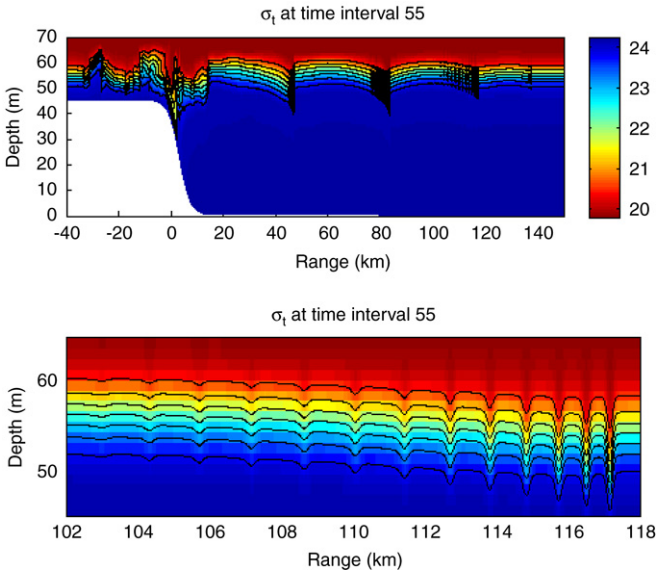

Fig. 10. Case 7 in Table 2. The shelf depth is 25 m instead of 15 m as in case 1. Predicted density field at 55 h. Upper panel shows predicted density structure. Lower panel shows an expanded view of second solitary wave train. As the shelf depth is lowered, number of solitary waves and their amplitudes tend to decrease relative to case 1.

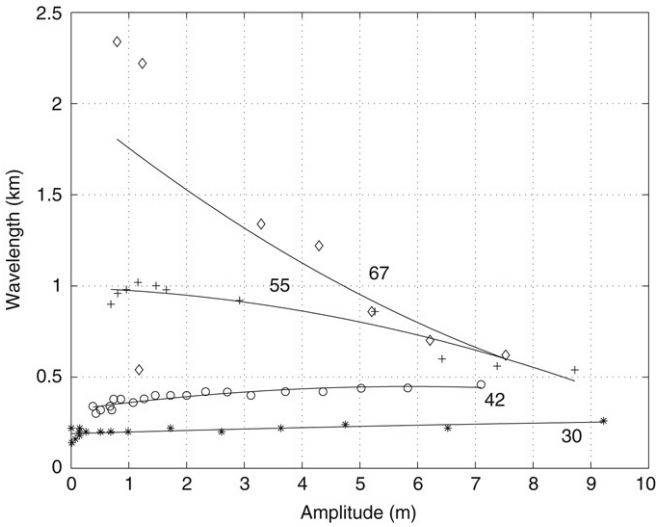

Fig. 11. Amplitude–wavelength dispersion diagram for case 1 in Table 1 at 30, 42, 55 and 67 h.

the wavelengths and amplitudes decrease from the front to the back of the train. At 55 h the structure of the soliton train changes, whereby the wavelengths tend to increase from the front to the back of the train with the amplitudes decreasing as before. The wavelength variation is from 550 to 1000 m. The wavelength behavior is indicative of a dispersion regime change. At 67 h the amplitudes decrease, as before, and the wavelengths show more increase than at 55 h from front to back, ranging from 625 to 2300 m. At the back of the soliton train the distances between the centers of the depression increase appreciably as evidenced in Fig. 4. The 55 and 67 h dispersion behavior belong to regime B, Section 2, where the wavelengths increase from front to back of the train and the amplitudes decrease. The solitons in the trains evolve from regime A to regime B.

5. Conclusion

A modeling study shows that, as the semidiurnal barotropic tide moves back and forth over the shelfbreak in the Shandong area of the Yellow Sea, generation of internal bores occurs. The internal bore depressions result in right and left propagating waves. The propagating depression waves steepen through nonlinear effects and disintegrate into solitary

waves through frequency and amplitude dispersions. Internal solitary wave train propagating away from the shelfbreak are generated. The generation occurs every semidiurnal tidal cycle.

We applied a scaling analogue of a two-layer system to the predicted numerical solutions with the full nonlinear nonhydrostatic Lamb [3] model. We calculated parameters of pycnocline density difference, linear phase speed, Froude number, nonhydrostatic dispersion, topographic length scale, tidal excursion distance, topographic height, and nonlinearity. Variations of density difference across the pycnocline, tidal forcing and topographic height were undertaken relative to a reference case tuned to data.

As density difference across pycnocline increases, the phase speed increases and nonhydrostatic dispersion parameter and Froude number decrease, Table 2. The nonlinearity and topographic height parameters remain the same. Their magnitude is approaching one and suggests appreciable topographic changes and nonlinear effects. As the density difference across pycnocline decreases, the phase speed decreases, nonhydrostatic dispersion parameter and Froude number increase. For the lowest density difference across the pycnocline, case 5 in Table 2, a profound change in predicted density structure occurs. Solitary waves do not evolve. Instead there are small internal tide depressions that propagate to the right. An internal tide type of configuration results from these particular parameters.

A decrease in barotropic tidal forcing, leads to a decrease in Froude number, tidal excursion, and nonlinearity parameters. There are fewer evolved solitons in the trains with smaller amplitudes.

As the topographic height parameters are decreased from 55 to 45 m, the topographic height and nonlinearity parameters decrease relative to case 1 (reference case). The number of solitary waves decrease in the trains and the amplitudes become smaller.

Dispersion diagrams of wavelength and amplitude indicate confinement of dispersion to parts of the diagram. The oceanographic parameters associated with the confinement areas of dispersion will be related in Part B of this study to acoustical parameters that cause transmission loss at certain frequencies. A feedback loop will be established between oceanographic and acoustical parameters.

Acknowledgments

We gratefully acknowledge the many helpful comments made by colleagues. The work was supported by the Office of Naval Research under PE 62435, with technical management provided by the Naval Research Laboratory.

Appendix. Nonhydrostatic Lamb model

The Lamb [3] model is used for simulating the generation and propagation of internal solitary waves in the Shandong area of the Yellow Sea, Fig. 1. It is a fully nonlinear and nonhydrostatic model. It consists of the incompressible Boussinesq equations on a rotating f plane. In the along-bank direction (i.e., y-direction), the velocity v is included but the derivatives with respect to the y-coordinate are neglected (hence, the designation "2.5 dimensional" representation). The equations of the model are:

$$V_t + V.\nabla V - fV \times \vec{k} = -\nabla p - \vec{k}\rho g, \tag{1}$$

$$\rho_t + V \cdot \nabla\rho = 0, \tag{2}$$

$$\nabla \cdot V = 0, \tag{3}$$

where viscosity is neglected, $V\ (u, v, w)$ is the velocity vector, ∇ is the three-dimensional vector gradient operator, subscript t denotes the time derivative, ρ has been scaled by the reference density as well as P after the hydrostatic pressure in balance with ρ_0 has been subtracted off, i.e., the physical density is $\rho_0(1 + \rho)$, and the physical pressure is $\rho_0(p - gz)$, g is the gravitational acceleration, f is the Coriolis parameter taken as 9.029×10^{-5} s^{-1}, and $\hat{k}$ is the unit vector along the z-direction. In the three-dimensional equations (1) to (3) the partial derivatives with respect to y are neglected, i.e. $\partial/\partial y(.) = 0$. Thus, Eqs. (1) to (3) are equivalent to Equations (1a) to (1d) in Lamb's [3] paper. The y-component $v(x, y)$ of the model is in geostrophic balance with the horizontally varying density field.

Before the equations are solved, they are transformed to a terrain following coordinate system (sigma-coordinates) in the vertical, which leads to higher vertical resolution over the sill of the strait. The equations are solved on a domain bounded below by the topography at $z = h(z)$ and above by a rigid lid. There is no normal flow at the upper and lower boundaries. H is the deep-water depth. The right boundary is treated as an outflow, tidal forcing is applied on the left boundary.

References

[1] A. Warn-Varnas, S.A. Chin-Bing, D.B. King, J.A. Hawkins, K.G. Lamb, M. Teixeira, Yellow Sea ocean-acoustic solitary wave modeling studies, J. Geophys. Res. 110 (2005) C08001, doi:10.1029/2004JC002801.
[2] M. Teixeira, A. Warn-Varnas, J. Apel, J. Hawkins, Analytical and observational studies of internal waves in the Yellow Sea, J. Coastal Res. 22 (6) (2006) 1408–1416.
[3] K. Lamb, Numerical experiments of internal waves generated by strong tidal flow across a finite amplitude bank edge, J. Geophys. Res. 99 (c1) (1994) 848–864.
[4] J.R. Apel, A new analytical model for internal solitons in the ocean, J. Phys. Oceanogr. 33 (11) (2003) 2247–2269.

[5] A.R. Osborne, M. Serio, L. Bergamasco, L. Cavaleri, Solitons, cnoidal waves and nonlinear interactions in shallow-water ocean surface waves, Physica D 123 (1998) 64–81.
[6] J.A. Hawkins, A. Warn-Varnas, I. Christov, Fourier, scattering and wavelet transforms: Application to internal gravity waves with comparisons to linear tidal data, in: R.V. Donner, S.M. Barbosa (Eds.), Nonlinear Time Series Analysis in the Geosciences, Springer, 2008, pp. 223–244.
[7] J.X. Zhou, X.Z. Zhang, P.H. Rogers, Resonant interaction of sound wave with internal solitons in coastal zone, J. Acoust. Soc. Am. 90 (4) (1991) 2042–2054.
[8] S.A. Chin-Bing, D.B. King, J.E. Murphy, Numerical simulations of lower frequency acoustic propagation and backscatter from solitary internal waves in a shallow water environment, in: D.D. Ellis, J.R. Preston, H.G. Urban (Eds.), Ocean Reverberation, Kluwer Academic Press, Dordrecht, The Netherlands, 1993.
[9] D.B. King, S.A. Chin-Bing, R.W. McGirr, Effect of shallow water internal waves on broadband acoustic wave propagation, in: D. Lee, M. Shultz (Eds.), Environmental Acoustics: International Conference on Theoretical & Computational Acoustics Vol. II, World Scientific Press, Singapore, 1994, pp. 793–808.
[10] A. Warn-Varnas, S.A. Chin-Bing, D.B. King, J.A. Hawkins, K.G. Lamb, M. Teixeira, Yellow Sea internal solitary wave variability, in: N.G. Pace, Finn B. Jensen (Eds.), Impact of Littoral Environmental Variability on Acoustic Predictions and Sonar Performance, Kluwer Academic Publishers, Dordrecht, The Netherlands, 2002.
[11] T. Gerkema, Nonlinear dispersive internal tides: Generation models for a rotating ocean, Doctoral Thesis, Royal Netherlands Institute for Sea Research, Texel, The Netherlands, p. 149.